Self-Assembling, Bioinspired Wax Crystalline Surfaces with Time-Dependent Wettability

*Sasha Pechook and Boaz Pokroy**

One of the most fascinating properties of materials in nature is the superhydrophobic and self-cleaning capabilities of different plant surfaces. This is usually achieved by the hydrophobic cuticles that are made of cutin and contain wax crystals both within them and on their surfaces. Here, bioinspired *n*-hexatriacontane wax films are deposited via thermal evaporation and it is shown that the surface evolves in time via self-assembly. This leads to a dramatic change in the wetting properties with a transition from hydrophobic to superhydrophobic characteristics, which takes place within several days at room temperature. This phenomenon is investigated and strain-induced recrystallization is proposed to be the mechanism for it. This work could become the basis for the inspiration and production of tuned, time-dependant, temperature-sensitive, variable-wettability surfaces.

1. Introduction

Nature is replete with materials that exhibit properties tailored to specific functions. Some examples are mollusk shells and bone, which exhibit superior mechanical properties,[1] the brittle star and venus basket, which exhibit beautiful optical properties,[2,3] magnetotactic bacteria, which have outstanding magnetic properties,[4] and different plants, which exhibit superhydrophobic and self cleaning surface properties.[5]

This latter phenomenon was observed in nature decades ago, particularly among insects such as butterflies and a range of land plants including wheat, taro, cabbage, and several others.[6] The best-known example is the lotus leaf.[7] Most higher species of land plants are composed of hydrophobic cuticles made of cutin-containing wax crystals within them and on their surfaces.[8] It has been shown that the natural waxes, which are located on the surface of the cuticle, can exhibit several different morphological forms such as platelets, tubules, rodlets, threads, and others.[9] These epicuticular waxes have a hierarchical roughness that, combined with their intrinsic hydrophobic characteristics, results in superhydrophobic qualities that exist on the surface of the leaves. In many cases this enables the plants to reduce water loss, reduce debris adhesion (self cleaning), and reduce the adhesion of pathogens.

S. Pechook, Dr. B. Pokroy
Department of Materials Engineering and Russell Berrie Nanotechnology Institute
Technion - Israel Institute of Technology
Haifa 3200, Israel
E-mail: bpokroy@tx.technion.ac.il

DOI: 10.1002/adfm.201101721

Superhydrophobicity originates in the roughness of an intrinsic hydrophobic surface[10–13] and cannot be generated solely by surface chemistry. It is the combination of the hydrophobicity of the wax on plant surfaces and their roughness due to the crystal shapes that generate the superhydrophobicity that characterizes their leaves.

Over the last two decades there have been many studies in which biomimetic counterparts were fabricated.[14–16] In most of these studies at least two different components where utilized, namely a texture, which introduces the surface roughness, and a surface treatment, which introduces the intrinsic hydrophobic nature (surface chemistry). Using such an approach, it has been shown that one can not only produce superhydrophobic surfaces that also exhibit self-cleaning properties but moreover that also exhibit superlyophobic,[17] superomniphobic,[18] and even anti-icing properties.[19–21]

There are only a few bioinspired studies in which wax crystals have been employed in a one-step production so that they serve both as the chemical element and as the roughness element. Koch et al., in their pioneering work, extracted natural waxes from the leaf of wheat and grew crystals of these waxes mainly from solution but also by thermal evaporation on different surfaces.[22,23] They showed that such waxy surfaces do indeed exhibit high roughness similar to that which was observed in the biological counterpart. Others have used thermal evaporation of *n*-hexatriacontane ($C_{36}H_{74}$) and shown that this also produces superhydrophobic surfaces.[24] Bhushan et al. further developed this by combining thermal evaporation of *n*-hexatriacontane with micropatterned epoxy replicas as substrates so as to gain several orders of hierarchy, which increased the superhydrophobicity of the surface.[25]

Here, we show that the nanoroughness of the thermally deposited *n*-hexatriacontane wax surface evolves in time via self assembly and this leads to a dramatic change in the wetting properties with a transition from hydrophobic to superhydrophobic characteristics. We investigated this phenomenon and propose a mechanism for it.

2. Results and Discussion

In order to investigate the time-dependent nanoroughness of thin wax films and its effect on the wetting properties, ≈100 nm thick films of crystalline *n*-hexatriacontane (*n*-hexatriacontane

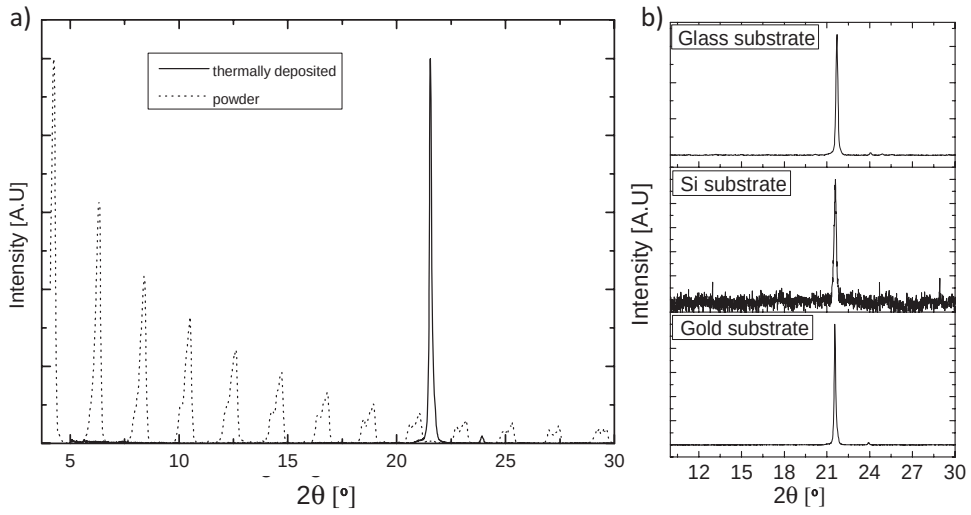

Figure 1. a) XRD spectrum of $C_{36}H_{74}$ powder sample (dashed line) and thermally deposited film on gold (black line). In the case of the thermally deposited sample, a strong (110) preferred orientation can be seen at 2 θ of 21.6°, and a minor peak of the (200) plane present at 23.9°. b) XRD spectrum of thermally deposited $C_{36}H_{74}$ film on gold, glass, and Si substrates the strong (110) preferred orientation is observed at 2 θ of 21.6° for all substrates. Diffraction was carried out with Cu Kα.

has an orthorhombic crystal structure[26,27]) were thermally evaporated on different substrates (a silicon wafer, a glass slide, a thin layer of gold on silicon, and on a 1-undecanethiol self-assembled monolayer (SAM) supported on gold). After deposition on each of these substrates we performed powder X-ray diffraction (XRD), high-resolution scanning electron microscopy (HRSEM), and optical confocal imaging of the surfaces.

A striking observation by XRD was the extremely high preferred orientation of all the wax films deposited. This preferred orientation was observed from the very start and increased with time and can be observed in **Figure 1**a. It is interesting to note that the same preferred orientation was observed for all samples with no dependence on the substrate type (Figure 1b). Using the Joint Committee on Powder Diffraction Standards (JCPDS) card for this structure (PDF #38-1975) we found the position of the preferred orientation diffraction peak. This peak was clearly of the (110)-type. There is one additional small diffraction peak, which is derived from the (200) plane.

Using a recent extension of the March–Dollase method,[28] one can estimate the degree of preferred orientation as:[29] $\eta = 100\%\left[(1-r)^3/(1-r^3)\right]^{1/2}$, where $r = \left[\sin^2\alpha/((\kappa/\kappa_p)^{2/3} - \cos^2\alpha)\right]^{1/3}$; α is the angle between the plane of preferred orientation and a comparison plane, and k and k_p are the observed and random powder intensity ratios between the two planes under consideration, respectively.

We derived that the percentage of preferred orientation of a film immediately after being deposited is 86%, which is very high. However after 113 h at room temperature we derived it to be 92% and when the samples were aged at a temperature of 40 °C overnight we found that the degree of preferred orientation rose to the fantastic figure of 99.5% and was not substrate dependent.

In parallel to the strong change in preferred orientation, we also performed time-dependent water wettability measurements by measuring the contact angle of a water drop on the surface (sessile drop measurement). Indeed we found a dramatic change from being hydrophobic, for the immediately deposited samples, to being superhydrophobic for the aged samples (**Figure 2** and Supporting Information Figure S2). This indicated that the change in preferred orientation was accompanied by some change in the crystal morphology and shape, which in turn led to nanoroughening of the surface. We used in situ time-resolved confocal microscopy and observed the change in surface roughness over a constant 100 μm × 100 μm area for a duration of 160 h. We collected a topographical image every hour (**Figure 3**), which can also be seen as a time-dependent movie (Supporting Information Movie S1). The root mean square (R.M.S.) roughness changed from ≈5 nm for the as deposited film to ≈180 nm after 160 h at room temperature (Figure 3 and **Figure 4**). The increase in roughness of an

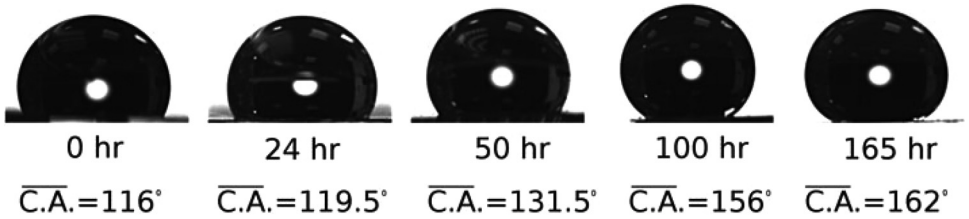

Figure 2. Time-dependant contact angle measurements of a 7 μL water droplet on thermally deposited *n* -hexatriacontan on a gold substrate.

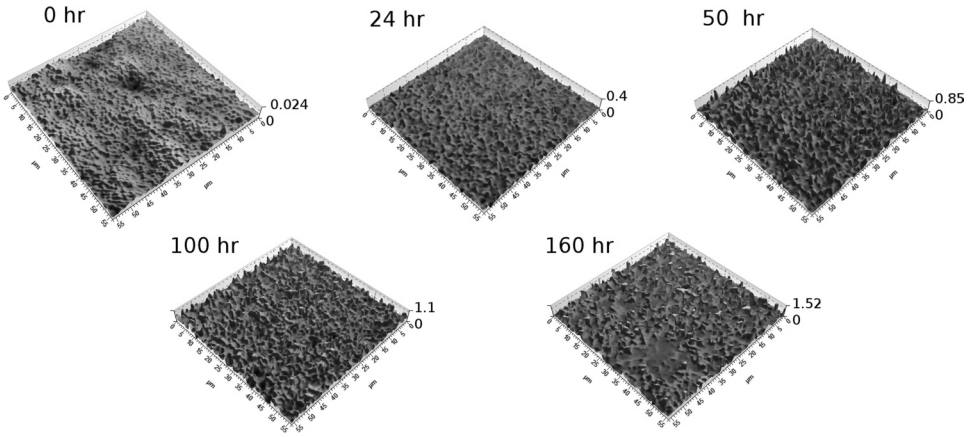

Figure 3. Accorded time-dependent confocal images showing the roughness of the wax-coated gold surface. The axes' units are in μm.

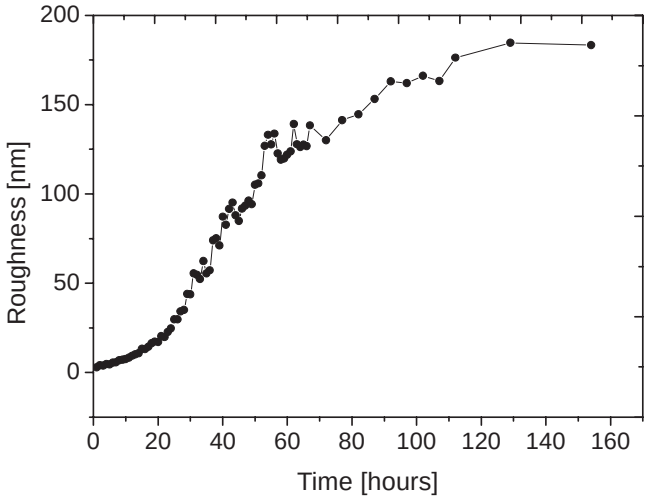

Figure 4. R.M.S. roughness of the wax-coated gold surface as a function of time, as measured by confocal microscopy.

intrinsically hydrophobic surface should undoubtedly lead to an increase in the hydrophobicity of the surface, as can be clearly seen from the Cassie and Baxter equation,[30] $\cos\theta = R_f\cos\theta_0 - f_{LA}(R_f\cos\theta_0 + 1)$, where θ_0 is the contact angle for a smooth surface and $R_f > 1$ is the roughness factor, which is defined as $R_f = A_{SL}/A_F$ where A_{SL} is the ratio of the solid–liquid area and A_F is the projection of A_{SL} on a flat plane, and f_{LA} is the fractional flat geometric area of the liquid–air interfaces under the droplet. Time-dependent HRSEM revealed the shift from an almost conformal film to a strongly faceted array of distinct single crystal platelets of wax (**Figure 5** and **Figure 6**). These platelets are only 50–200 nm thick and seem to be mostly standing perpendicular to the substrate. Such platelets were observed on all the examined substrates (Supporting Information Figure S1). This is what imparts the high roughness and, in turn, the superhydrophobic characteristics to the surface. The morphology of these crystals as faceted platelets fits well with what was previously noticed for the case of thermally deposited *n*-hexatriacontane[27] (Figure 6). According to that work, the wax molecule backbone

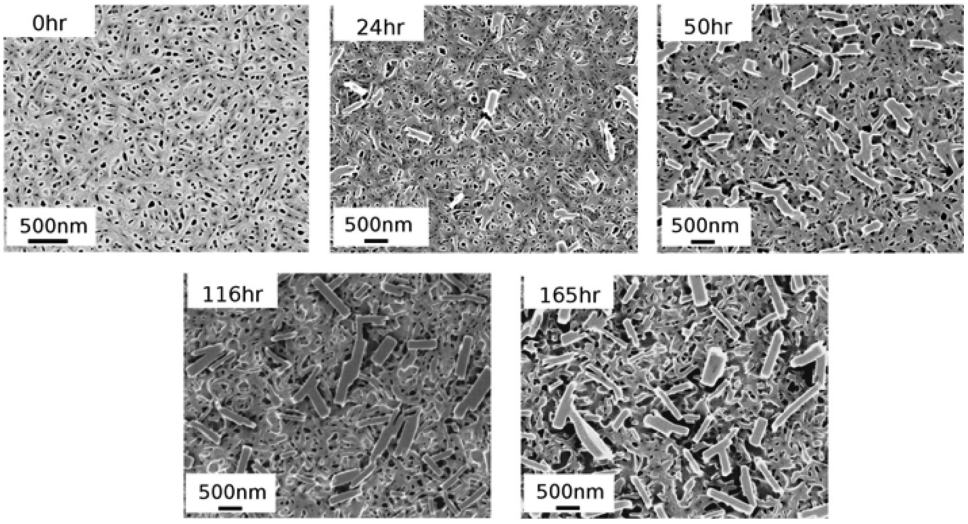

Figure 5. Accorded time-dependent HRSEM images showing the wax crystals on a gold surface.

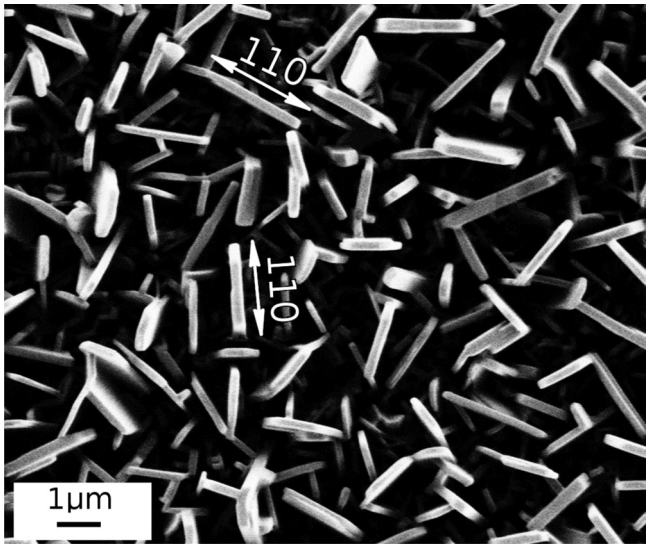

Figure 6. HRSEM image showing the faceted wax crystals on a gold surface aged for three days at room temperature. Arrows indicating the top facet, which is the (110)-type.

lies perpendicular to the wax crystal platelet. Comparing the morphology observed previously[27] we can see nice agreement with the XRD data, which indicates the (110) plane to be the nucleation plane.

In the quest to understand the mechanism by which the wax crystals grow at room temperature, we performed in situ XRD over 50 h at room temperature and repeated the time-dependent wetting and roughness testing for samples that were maintained at various temperatures (–30 °C, 4 °C, and 40 °C). From the XRD data for the room-temperature samples (**Figure 7**a) we could observe a clear shift in the position of the (110) diffraction peak from higher to lower 2θ diffraction angles. We could calibrate the peak position by using the position of the single crystal silicon substrate and/or the gold layer. The peak shift corresponds to a relaxation of an initial compressive strain due to the deposition. It is well known that thermal evaporation of thin films at room temperature introduces strains into the films.[31] In order to calculate the strain, ε, from the shift of the diffraction peak we used the well-know equation: $\varepsilon = (d_m - d_0)/d_0$, where d_m and d_0 are the measured d-spacing and the unstrained d-spacing, respectively.[32] It was found that the strain of the as-deposited film was ≈1%. In parallel the rate of roughening, which corresponds to crystal recrystallization, increased with temperature but was completely halted at –30 °C (Figure 7b). When samples were taken out of this temperature and placed at room temperature which is not far from the wax melting temperature, T_m, (≈0.86 T_m, T_m = 347 K), surface roughening took place, but when placed back at –30 °C the growth was halted again. At an intermediate temperature of 4 °C (≈0.8 T_m) the roughening occurs at a low rate. These two observations, combined with the sigmoid shape of the roughness versus time curve (Figure 4) and the absence of an amorphous phase after the film deposition, strongly indicate that the mechanism of increase in surface roughness is recrystallization.[33] The driving force for recrystallization is the compressive strain induced by the relatively rapid deposition method. This is very similar to recrystallization in metallurgy, where the driving force is the deformation energy stored in the metal in the form of dislocation strain fields. In the case of wax the driving force is the deformation strain energy due to the deposition procedure itself. The driving force for recrystallization can be seen as force acting per unit area on the grain boundaries (units of N m^{-2}), i.e., as a pressure on the grain boundary.[33] This leads to the formation of new crystals from old ones, which are free from strain and which have much lower defect densities.

Alongside with the time-dependent strain relaxation we also determined the time evolution of the grain size. Crystallite size determined from the broadening of the XRD diffraction peaks (i.e.,the size of coherently scattering blocks) was calculated according to[34] $L = 2d(\tan\theta_B)/W_L$ where W_L is the Lorentzian width of the diffraction peak, d is the d-spacing that correlates to the diffraction peak, and θ_B is the Bragg diffraction angle. It was found that the average crystallite size of the as deposited sample was 81 nm ± 3 nm and after 50 h grew to 139 nm ± 5 nm (Supporting Information Table S1). In order to obtain the Lorentzian contribution to the diffraction peak we fitted the peak profile to a Voigt function, which is a convolution of a Gaussian and a Lorentzian.[34] This increase of the crystallite size is yet another evidence of recrystallization as the perfect domain (defect-free) size increases with time.

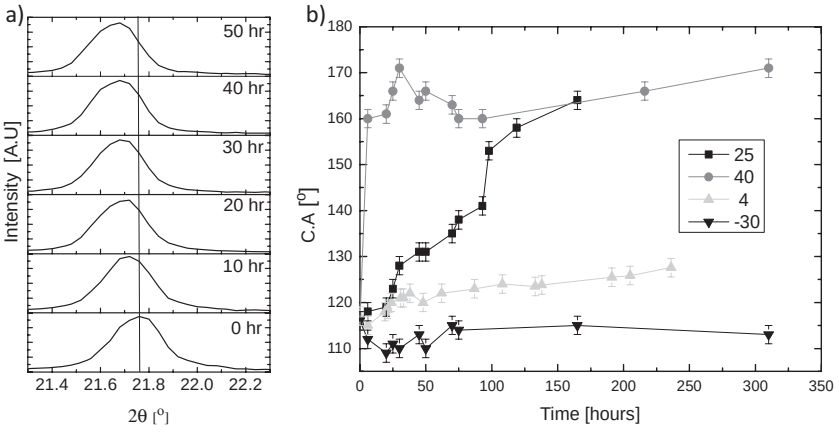

Figure 7. a) Time-dependent XRD measurements over 50 h with 1 h intervals showing the (110) diffraction peak. b) Contact angle (C.A.) as a function of time for substrates maintained at four different temperatures: deep-freeze (–30 °C), upside down triangles; refrigerator (4 °C), triangles; room temperature (25 °C), squares; and in the oven (40 °C), circles. The samples were evaporated on gold surfaces.

Additional evidence for this phenomenon in our case can be found in the results of the confocal measurements, which demonstrated significant crystal growth over time, from the initial value of 24 nm to 1.52 μm after 165 h at room temperature, in addition to a corresponding increase in the surface roughness. HRSEM images support the X-ray and confocal experiments (Figure 5). We stress that the sizes derived by microscopy and from XRD do not necessarily match, as the perfect

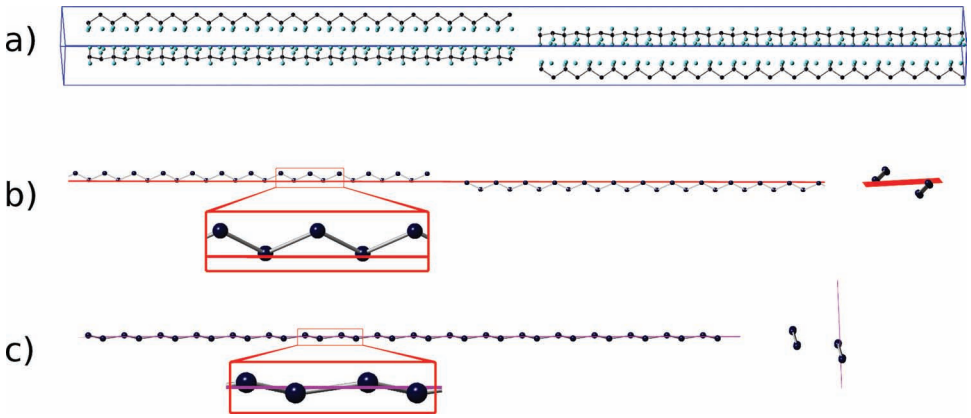

Figure 8. Crystal structure of orthorhombic *n* -hexatriacontane. a) Unit cell oriented so that the (110) plane is in the plane of the page. b) Part of a unit cell showing the (200) plane in red. The image on the right is a magnification of a small section showing the relation between the (200) plane and the carbon–carbon bonds. c) Part of a unit cell showing the (110) plane in magenta. The image on the right is a magnification of a small section showing the relation between the (100) plane and the carbon–carbon bonds.

domain size derived by the latter is almost always smaller than the physical size of the crystals. A similar mechanism was observed, for example, in metallic thin films such as electron-beam-deposited Pt films.[35]

A challenging question was, "Why is the preferred orientation we observed that of the (110) plane and the minor one that of the (200) plane?" For this purpose we built the crystalline unit cell of *n*-hexatriacontane and observed the two specific planes. In **Figure 8** one can see that the (110) plane is a plane that is parallel to the wax carbon backbone but in addition it is the plane in which most of the carbon–carbon bonds lie. This probably implies that when one evaporates the wax and deposits it kinetically on a surface, the long wax molecules do not have time to reorganize. It is probably energetically preferable to nucleate the crystals via the (110) plane, as this allows for a maximum number of carbon atoms from the backbone to be on the template surface. The second plane that is observed to some extent but much less is the (200). This plane is also parallel to the carbon backbone however does not contain the carbon–carbon bonds and is rather at an oblique angle to these bonds (Figure 8b,c). This is probably why it is less favorable. We believe that this geometric explanation can clarify not only the specific nucleation plane but also the reason why the preferred orientation is not substrate-dependent and is extremely high. Performing an XRD rocking curve demonstrated a very narrow peak of only 2.9°, which means that the spread of the orientation of the crystals is extremely narrow. We believe that if the deposition rate could be controlled and kept at a much lower rate we would see a much lower degree of preferred orientation, which, in turn, would be template-affected and the wax crystals would have less strain.

With regards to the high aspect ratio of the wax crystallite tablets, we refer to Fu et al.[36] where it was shown that the van der Waals forces between adjacent backbone chains are much stronger than the interaction between the tails of the chains. This leads to a self-assembly mechanism of growth and therefore to a much faster growth rate perpendicular to the chains. Since the chains are perpendicular to the face of the tablets one can understand why these tablets are so anisotropic in shape.

3. Conclusions

We have shown that bioinspired wax surfaces with nanoroughness exhibit room-temperature, time-dependent nanostructure evolution. We found that a thin wax layer deposited by thermal evaporation is rather highly strained, which serves as the driving force for recrystallization. The latter leads to the spontaneous increase in roughness (from nanometer-sized to micrometer-sized wax crystals), which in turn leads to the transition of the film from exhibiting hydrophobic to superhydrophobic characteristics. We have characterized this phenomenon and have been able to identify the underlying mechanism for it.

We believe that this work could become a basis for the inspiration and production of tuned, time-dependent, temperature-sensitive, variable-wettability surfaces. In addition we also believe that the mechanism presented in this work could possibly explain the self-assembly formation of nanoroughened superhydrophobic wax surfaces in nature.

4. Experimental Section

Sample Preparation: The films were prepared via self-assembly of *n*-alkane hexatriacontane paraffin wax ($C_{36}H_{74}$) (purity 98%, Sigma-Aldrich, France). The wax was deposited by thermal evaporation via a Bio-Rad Polaron Division Coating System on different substrates: 200 nm gold films modified with 1-undecanethiol ($CH_3(CH_2)_{10}SH$) SAMs (purity 98%, Sigma-Aldrich, France), (100) silicon wafers, and microscope glass slides. The samples were placed in a vacuum chamber at 10^{-4} mbar on a holder placed 10 to 12 cm above a crucible loaded with 40 to 50 mg of *n*-hexatriacontane wax. The wax was evaporated at a crucible temperature of ≈200 °C by applying pulses of an electrical current. After evaporation, the specimens were placed at different temperatures: 25 °C (room temperature (R.T.)), 4 °C (refrigerator), –30 °C (deep-freeze), and 40 °C (MRC-1410DIG oven, in air).

Characterization: The wettability of the surfaces was characterized using contact angle measurements recorded with an Attension Theta tensiometer. The measurements were performed during a 165 h period for the R.T. sample, a 240 h period for the 4 °C sample, and a period of 310 h for the samples kept at 40 °C and –30 °C. The wettability measurements were performed with a constant high-purity water drop volume of 7 µL.

Structural and microstructural characterization of the wax powder and crystalline thin films were performed by means of XRD with a Cu anode sealed tube (Philips PW 3710 X-Ray Diffractometer) performing single and time-dependant batch scans. Time-resolved X-ray measurements were performed for the duration of 3 days at 1 h intervals.

Surface imaging was performed using SEM (FEI E-SEM Quanta 200), HRSEM (Zeiss Ultra plus HR-SEM) and optical (Olympus BX51microscope and Olympus equipped with an Olympus SC30 camera) microscopy images were recorded at different times after deposition of the R.T samples. Confocal microscopy (Leica DCM3D) was used for time-dependent roughness observation. Time-dependent measurements were performed on counterpart samples that were used for XRD time-dependent measurements. These experiments encompassed the same duration and time intervals as the time-dependent XRD.

Supporting Information

Supporting Information is available from the Wiley Online Library or from the author.

Acknowledgements

The authors thank Dr. Michael Kalina from the Department of Materials Engineering at the Technion for help with the deposition and Prof. L. J. Gauckler from the ETH Zurich for helpful discussions.

Received: July 25, 2011
Revised: October 12, 2011
Published online: December 13, 2011

[1] J. W. C. Dunlop, R. Weinkamer, P. Fratzl, *Mater. Today* **2011**, *14*, 70.
[2] V. C. Sundar, A. D. Yablon, J. L. Grazul, M. Ilan, J. Aizenberg, *Nature* **2003**, *424*, 899.
[3] J. Aizenberg, A. Tkachenko, S. Weiner, L. Addadi, G. Hendler, *Nature* **2001**, *412*, 819.
[4] S. Mann, N. H. C. Sparks, R. B. Frankel, D. A. Bazylinski, H. W. Jannasch, *Nature* **1990**, *343*, 258.
[5] K. Koch, H. F. Bohn, W. Barthlott, *Langmuir* **2009**, *25*, 14116.
[6] C. Neinhuis, W. Barthlott, *Ann. Bot.* **1997**, *79*, 667.
[7] W. Barthlott, C. Neinhuis, *Planta* **1997**, *202*, 1.
[8] C. E. Jeffree, *The Fine Structure of the Plant Cuticle. Vol. 23*. Blackwell Publishing Ltd., Oxford **2007**.
[9] K. Koch, B. Bhushan, W. Barthlott, *Soft Matter* **2008**, *4*, 1943.
[10] R. N. Wenzel, *Ind. Eng. Chem.* **1936**, *28*, 988.
[11] A. B. D. Cassie, S. Baxter, *Trans. Faraday Soc.* **1944**, *40*, 546.
[12] J. Bico, C. Marzolin, D. Quere, *Europhys. Lett.* **1999**, *47*, 220.
[13] D. Oner, T. J. McCarthy, *Langmuir* **2000**, *16*, 7777.
[14] G. S. Watson, B. W. Cribb, J. A. Watson, *ACS Nano* **2010**, *4*, 129.
[15] Y. C. Jung, B. Bhushan, *ACS Nano* **2009**, *3*, 4155.
[16] A. Tuteja, W. Choi, M. L. Ma, J. M. Mabry, S. A. Mazzella, G. C. Rutledge, G. H. McKinley, R. E. Cohen, *Science* **2007**, *318*, 1618.
[17] A. Ahuja, J. A. Taylor, V. Lifton, A. A. Sidorenko, T. R. Salamon, E. J. Lobaton, P. Kolodner, T. N. Krupenkin, *Langmuir* **2008**, *24*, 9.
[18] A. Tuteja, W. Choi, J. M. Mabry, G. H. McKinley, R. E. Cohen, *Proc. Natl. Acad. Sci. USA* **2008**, *105*, 18200.
[19] L. Mishchenko, B. Hatton, V. Bahadur, J. A. Taylor, T. Krupenkin, J. Aizenberg, *ACS Nano* **2010**, *4*, 7699.
[20] A. J. Meuler, G. H. McKinley, R. E. Cohen, *ACS Nano* **2010**, *4*, 7048.
[21] P. Tourkine, M. Le Merrer, D. Quere, *Langmuir* **2009**, *25*, 7214.
[22] K. Koch, W. Barthlott, S. Koch, A. Hommes, K. Wandelt, W. Mamdouh, S. De-Feyter, P. Broekmann, *Planta* **2006**, *223*, 258.
[23] A. Niemietz, K. Wandelt, W. Barthlott, K. Koch, *Progr. Org. Coat.* **2009**, *66*, 221.
[24] H. Tavana, A. Amirfazli, A. W. Neumann, *Langmuir* **2006**, *22*, 5556.
[25] B. Bhushan, Y. C. Jung, A. Niemietz, K. Koch, *Langmuir* **2009**, *25*, 1659.
[26] P. W. Teare, *Acta Crystallogr.* **1959**, *12*, 294.
[27] P. J. C. M. van Hoof, R. F. P. Grimbergen, H. Meekes, W. J. P. van Enckevort, P. Bennema, *J. Cryst. Growth* **1998**, *191*, 861.
[28] W. A. Dollase, *J. Appl. Crystallogr.* **1986**, *19*, 267.
[29] E. Zolotoyabko, *J. Appl. Crystallogr.* **2009**, *42*, 513.
[30] D. Quere, *Annu. Rev. Mater. Res.* **2008**, *38*, 71.
[31] J. A. Thornton, D. W. Hoffman, *Thin Solid Films* **1989**, *171*, 5.
[32] B. Pokroy, E. N. Caspi, J. P. Quintana, A. Berner, E. Zolotoyabko, *Nat. Mater.* **2004**, *4*, 900.
[33] G. Gottstein, *Physical Foundations of Materials Science,* Springer-Verlag, Berlin-Heidelberg-New York **2004**
[34] B. Pokroy, A. N. Fitch, E. Zolotoyabko, *Adv. Mater.* **2006**, *18*, 2363.
[35] H. Galinski, T. Ryll, P. Elser, J. L. M. Rupp, A. Bieberle-Hutter, L. J. Gauckler, *Phys. Rev. B* **2010**, *82*, 235415
[36] J. Fu, S. G. Urquhart, *Langmuir* **2007**, *23*, 2615.